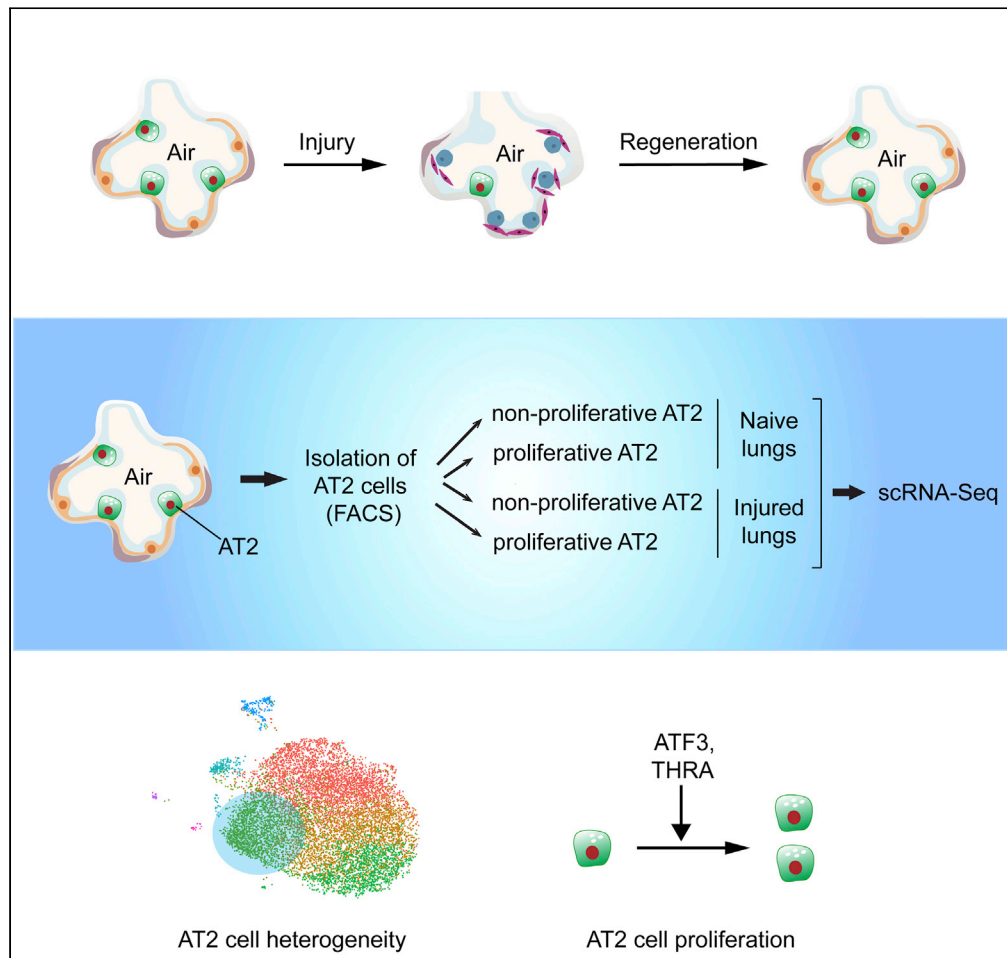# iScience

Article

Transcriptional responses to injury of regenerative lung alveolar epithelium

Mir Ali, Ryan LaCanna, Zhaorui Lian, ..., Wenna Shao, Xiang Yu, Ying Tian

ying.tian@temple.edu

Highlights

Alveolar epithelial type 2 (AT2) cells in mice are heterogeneous

ScRNA-seq identified a unique transcriptional program in proliferative AT2 cells

ATF3 and THRA factors exert proliferative functions in AT2 cells

Article

Transcriptional responses to injury of regenerative lung alveolar epithelium

Mir Ali,[1] Ryan LaCanna,[1,5] Zhaorui Lian,[2] Jian Huang,[2] Yinfei Tan,[3] Wenna Shao,[4] Xiang Yu,[4] and Ying Tian[1,6,*]

SUMMARY

The significance of alveolar epithelial type 2 (AT2) cell proliferation for lung alveolar epithelial homeostasis and regeneration after injury has been widely accepted. However, the heterogeneity of AT2 cell population for cell proliferation capacity remains disputed. By single-cell RNA sequencing and genetic lineage labeling using the Ki67 knock-in mouse model, we map all proliferative AT2 cells in homeostatic and regenerating murine lungs after injury induced by *Streptococcus pneumoniae* infection. The proliferative AT2 cell population displays a unique transcriptional program, which is regulated by activating transcription factor 3 (ATF3) and thyroid hormone receptor alpha (THRA) transcription factors. Overexpression of these two transcription factors in AT2 cells promoted AT2 cell proliferation and improved lung function after injury. These results indicate that increased expression of ATF3 and THRA at the onset of lung epithelial regeneration is required to permit rapid AT2 cell proliferation and hence progression through the recovery of lung epithelium.

INTRODUCTION

The adult mammalian lung epithelium possesses a unique ability to regenerate following various types of acute injuries (Hogan et al., 2014). In contrast, this regenerative capacity is lost in the lungs of aged mammals and the lungs of chronic obstructive pulmonary disease (COPD) (Navarro and Driscoll, 2017). Restoring the regenerative response of the lung epithelium in elderly and patients with COPD represents a possible treatment for lung repair, but a deeper understanding of the underlying mechanisms of regeneration is needed.

In mice, lineage tracing and lung injury models have demonstrated that alveolar epithelial type 2 (AT2) cells, that express surfactant protein C (SPC), play a major role in the maintenance of homeostasis and regeneration of the alveolar epithelium following various types of injury. Adult AT2 cells exhibit cell cycle re-entry and proliferate to replace lost tissue upon acute lung injury (Barkauskas et al., 2013). However, it is unclear whether all AT2 cells in adult lung have the ability to regenerate or if only a unique subset of AT2 cells performs this function. In addition, it is not clear whether there are molecular distinctions between regenerative and non-regenerative AT2 cells, and if so, what molecular mechanisms contribute to the AT2 regenerative response. To address this issue, we sought to generate an unbiased map of proliferative AT2 cell lineages in adult and injured mouse lungs. As the only defining characteristic of progenitor cells or stem cells is their ability to produce functional daughter cells through cell division (Clevers, 2015), we believe that the most unbiased way to indicate the involvement of AT2 progenitor cells in any biological growth or repair process is to genetically lineage label AT2 cells that proliferate during that related biological process. Although not present in the G0 phase, Ki67 is specially expressed in all actively cycling cells in the G1, S, G2, and M cell phases (Hutchins et al., 2010). Ki67 is widely used in developmental biology and pathology, as well as the application of general proliferation markers in clinical oncology (Whitfield et al., 2006). Here, we have generated $Ki67^{CreERT2}$; $Rosa26^{tdTomato}$; SPC^{EGFP} mice to identify proliferative AT2 cells in adult homeostatic and injured lungs. We used single-cell RNA sequencing to reveal distinct populations of proliferative AT2 cells in regenerating lung alveolar epithelium. We show that a distinct population of AT2 cells enters the cell cycle in response to injury. Transcriptome analysis of these AT2 cells revealed the gene regulatory network that supports the lung regenerative response. These basic studies may help us develop possible treatments to enter the process of lung alveolar epithelial repair and regeneration.

[1]Department of Cardiovascular Sciences, Center for Translational Medicine, Temple University Lewis Katz School of Medicine, Philadelphia, PA 19140, USA

[2]Coriell Institute for Medical Research, Camden, NJ 08103, USA

[3]Fox Chase Cancer Center, Temple University Health System, Philadelphia, PA 19111, USA

[4]Joint International Research Laboratory of Metabolic and Developmental Sciences, School of Life Sciences and Biotechnology, Shanghai Jiao Tong University, Shanghai 200240, China

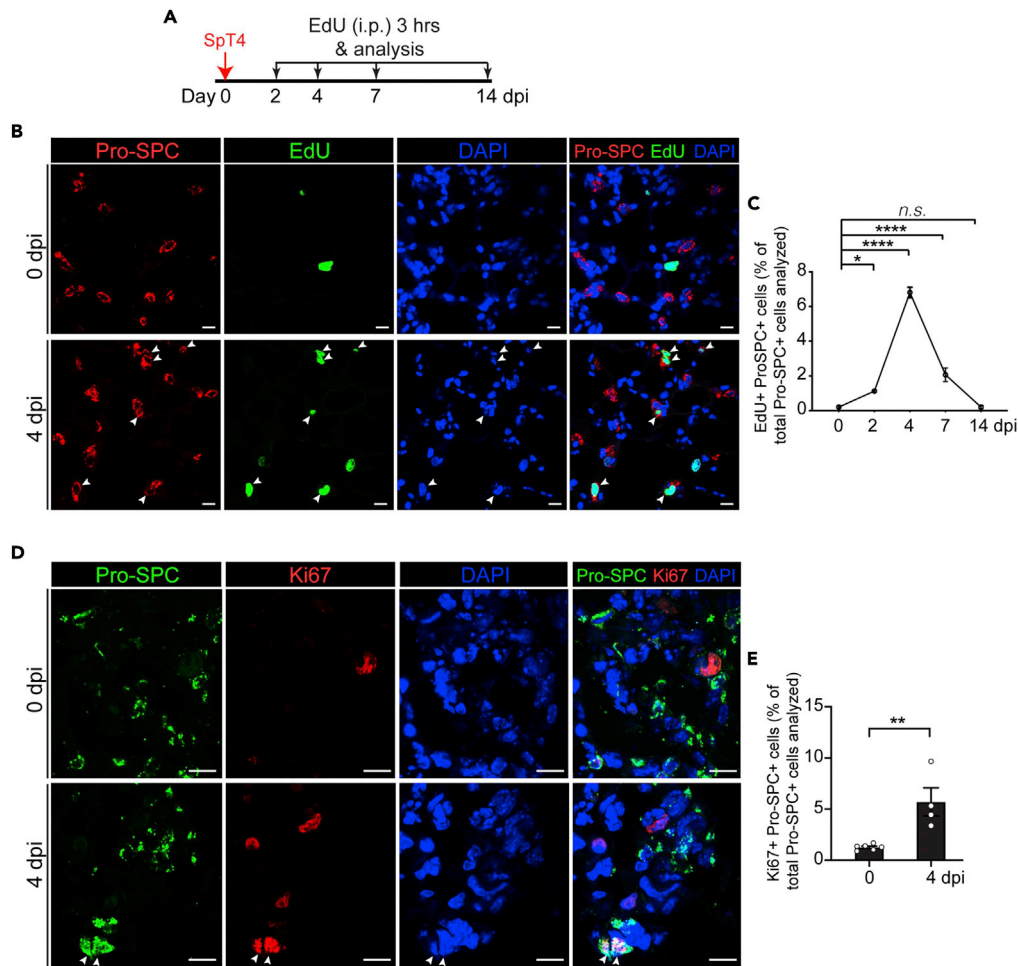[5]Present address: Department of Discovery Immunology, Genentech, South San Francisco, CA 94080

[6]Lead contact

*Correspondence:
ying.tian@temple.edu

https://doi.org/10.1016/j.isci.2022.104843

Figure 1. AT2 cell proliferation after SpT4 infection

(A) Schematic of experimental design. Wild-type adult mice were administrated with EdU via intraperitoneal (i.p.) injection (50 mg/kg), followed by a chase of 3 h.

(B) Confocal images of lung sections either before (0 dpi) or after (4 dpi) SpT4 infection. AT2 cells in the DNA synthesis phase were detected using Click-iT EdU Alexa Fluor (green) and co-immunostaining with antibody against Pro-SPC (red) to detect AT2 cells. Cell nuclear was stained with DAPI (blue). Arrows point to regions double-positive for Pro-SPC and EdU.

(C) Quantification of EdU + Pro-SPC + cells as the percentage of total Pro-SPC + cells analyzed (∼2200 Pro-SPC + cells per animal; four to six biological replicates per time point). (D) Confocal images of immunostained lung sections with antibodies to Pro-SPC (green) and Ki67 (red), a cell cycle marker, to detect proliferative AT2 cells. Arrows point to regions double-positive for Pro-SPC and Ki67.

(E) Quantification of the percentage of Ki67+Pro-SPC + cells of total Pro-SPC + cells analyzed. Scale bars: 10 μm in (B) and (D). Data are presented as mean ± SEM. *$p < 0.05$; **$p < 0.01$; ****$p < 0.0001$. p values were calculated using one-way ANOVA (C) and Student's t test (E). dpi: days post-infection.

RESULTS

Single-cell RNA-seq reveals different compositions of AT2 cells in regenerative lung alveolar epithelium

Our previous work shows that the sub-lethal infection of mice with *Streptococcus pneumoniae*, the most common pathogen of community-acquired pneumonia, led to exclusive damage in lung alveoli followed by alveolar epithelial regeneration (LaCanna et al., 2019; Wang et al., 2019). We show that SPC-expressing AT2 cells underwent proliferation and differentiation after *S. pneumoniae* strain T4 (SpT4) infection, which contributed to the newly formed alveolar epithelium (LaCanna et al., 2019). To determine DNA synthesis in AT2 cells, mice received a single intraperitoneal (i.p.) injection of 5-ethyl-2′-deoxyuridine (EdU) and were sacrificed after a 3-h labeling period (Figure 1A). The frequency of EdU incorporation was determined
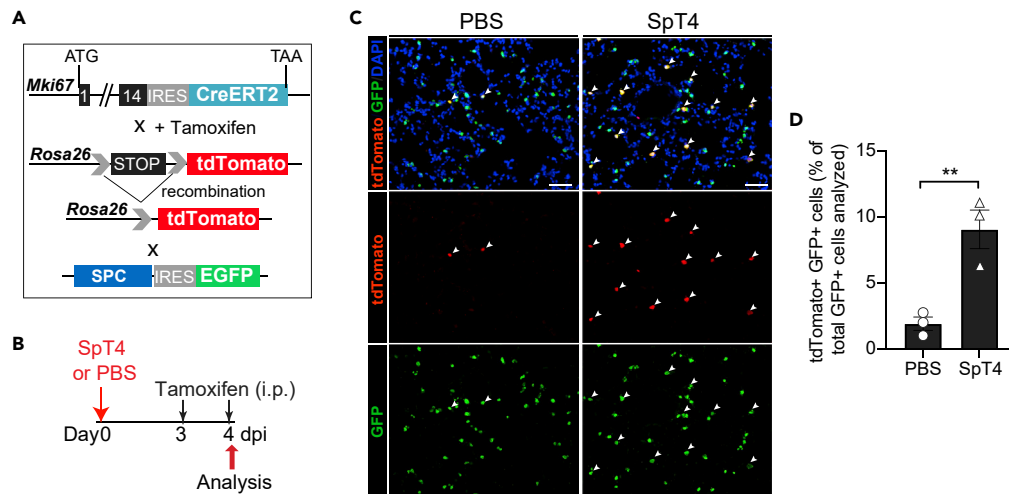
Figure 2. Genetic labeling of proliferative AT2 cells *in vivo*

(A) Schematic of experimental design for generating *Ki67^CreERT2^; Rosa26^tdTomato^; SPC^EGFP^* mice.

(B) Adult *Ki67^CreERT2^; Rosa26^tdTomato^; SPC^EGFP^* mice were administrated with tamoxifen at 3 dpi and 4 dpi. Four hours after the last dose of tamoxifen treatment, lungs were harvested for analysis.

(C) Immunostaining on lung sections with antibody against tdTomato/RFP (red) to detect lineage labeled Ki67 + cells and antibody against GFP (green) to detect SPC + AT2 cells. Arrows point to regions double-positive for tdTomato/RFP and GFP. Scale bars: 50 μm.

(D) Quantification of percentage of tdTomato + GFP + cells of total GFP + cells analyzed (mean ± SEM). **p < 0.01 (Student's t test).

on sectioned lungs by co-labeling with antibody against AT2 cells (Pro-SPC). A transient increase in DNA synthesis was observed in AT2 cells, with a peak labeling index of 7% ± 0.3% occurring at 4 days post-infection (dpi) (Figures 1B and 1C). The increased number of cycling AT2 cells in SpT4-infected mice was also observed by immunostaining of sectioned lungs for the cell cycle marker Ki67 (1.27% ± 0.12 vs. 5.70% ± 1.59%; 0 dpi vs. Four dpi, respectively; p < 0.01; Figures 1D and 1E).

To mark and capture proliferating AT2 cells in mouse lungs, we utilized a mouse model that expresses a tamoxifen-inducible version of the human estrogen receptor (Cre-ERT2), which is inserted downstream of the *Mki67* protein coding region (*Ki67^CreERT2^*) (Kretzschmar et al., 2018), and a mouse model that expresses an enhanced green fluorescent protein (EGFP) linked to the *SPC* protein (*SPC^EGFP^*) (Vanderbilt et al., 2015). We crossed *Ki67^CreERT2^* mice with *Rosa26^tdTomato^* reporter mice to generate *Ki67^CreERT2^; Rosa26^tdTomato^* mice. We examined the expression of Ki67 and RFP on naive lungs and found co-immunostaining of Ki67 and RFP after tamoxifen treatment (Figures S1A and S1B). There are 0.0% of Ki67 + cells showing spontaneous expression of Cre recombinase. In contrast, 89.25% ± 9.35% of Ki67 + cells show Cre recombinase after tamoxifen treatment (Figure S1C). The sensitivity and specificity of this lineage tagging system in our studies are consistent with other publications using this lineage tagging system (Kretzschmar et al., 2018). We then crossed *Ki67^CreERT2^; Rosa26^tdTomato^* mice with *SPC^EGFP^* mice to generate *Ki67^CreERT2^; Rosa26^tdTomato^; SPC^EGFP^* mice (thereafter Ki67-tdTomato, *SPC^EGFP^* mice; Figure 2A). Ki67-tdTomato, *SPC^EGFP^* mice at 10 weeks of age were administrated with intranasal inhalation of SpT4 or PBS. Lungs were analyzed on day 4 after infection. At 24 h (3 dpi) and 4 h (4 dpi) before harvesting the lung, tamoxifen was administered via i.p. injection (Figure 2B). AT2 cell proliferation was measured on sectioned lung tissues by co-immunostaining for the lineage-labeled proliferating cell marker (tdTomato/ RFP) and AT2 reporter (GFP) (Figure 2C). Mouse lungs subjected to SpT4 infection showed induced AT2 cell proliferation by 4 days after injury, suggestive of an acute regenerative response (LaCanna et al., 2019). By assessing the number of proliferating AT2 cells in regenerative lungs, we observed significant increases in the levels of AT2 cell proliferation (tdTomato + GFP+). On day 4 after SpT4 infection (4 dpi), the level of tdTomato + GFP+ was elevated by 14 ± 1.5-fold compared to that in the PBS-treated control lungs (Figure 2D). These results show that AT2 cells in adult mouse lungs entered the cell cycle in response to SpT4 infection-induced injury. The increased AT2 proliferation may regenerate alveolar epithelium.
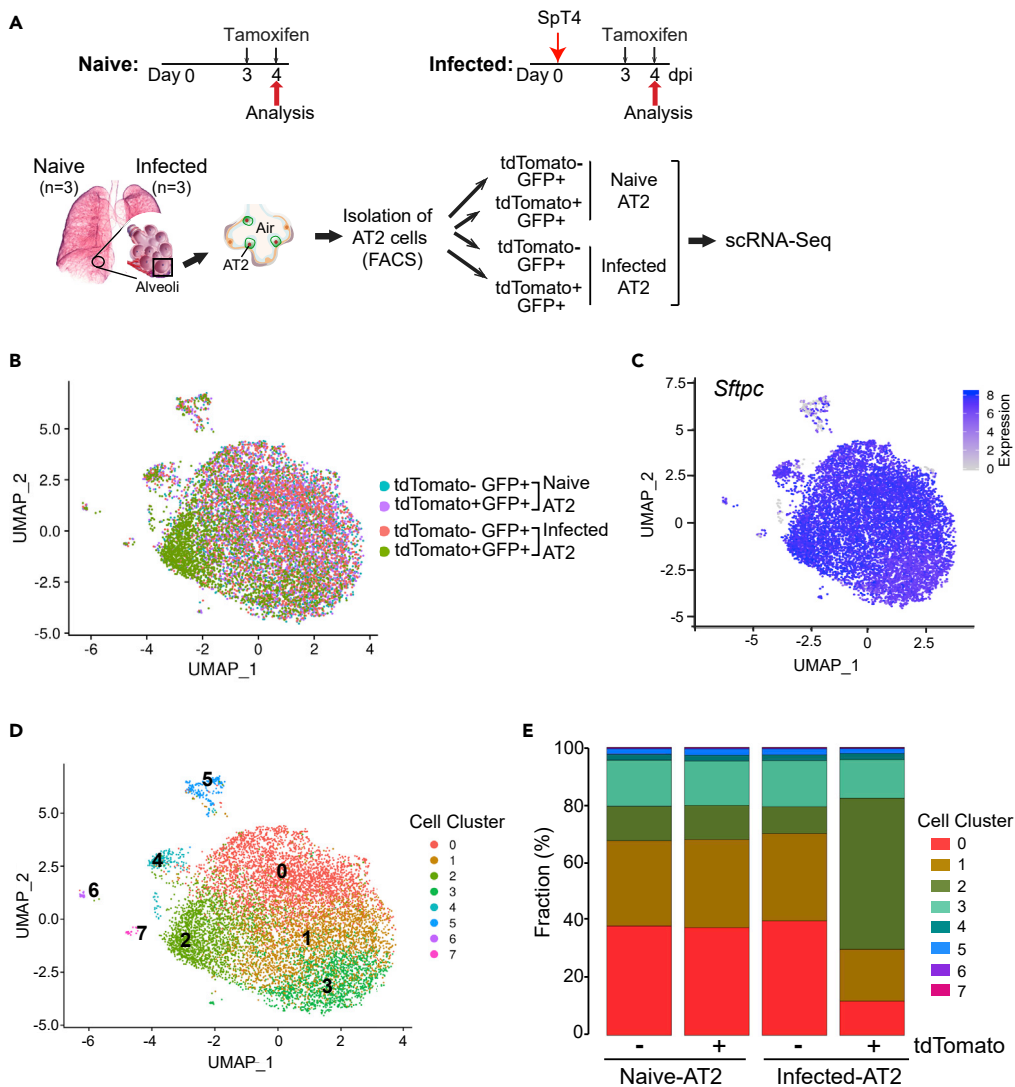
Figure 3. scRNA-seq identified distinct AT2 cell populations in the adult lungs

(A) Experimental design for scRNA-seq analysis. FACS, fluorescence-activated cell sorting.

(B) Uniform manifold approximation projection (UMAP) visualization of AT2 cell clusters colored by identity (n = 5,207 naive AT2 cells; n = 5,090 infected AT2 cells).

(C) Feature plot of *Sftpc* (*Spc*) expression in each AT2 cell cluster projected on UMAP graph.

(D) UMAP plots of AT2 cell clusters. Points are colored and numbered according to their computationally assigned cell type.

(E) Fraction of AT2 cell populations in each scRNA-seq sample.

To generate a comprehensive transcriptome atlas of proliferative AT2 cells during adult homeostasis and lung alveolar epithelial regeneration, we profiled proliferative AT2 (tdTomato + GFP+) and non-prolifera-tive AT2 (tdTomato-GFP+) cells at single-cell resolution. We isolated AT2 cells by dispase digestion and fluorescence-activated cell sorting (FACS) and performed scRNA-seq on AT2 cells of regenerative lungs 4 days after SpT4 infection (4 dpi) and on AT2 cells of naive lungs (Figure 3A). We captured 10,297 GFP + AT2 cells from all four samples with high integrity (Figures 3B, 3C, and S2). Given the analysis of RNA, 69% of unique molecular identifiers (UMIs) were mapped to exons and 12% were mapped to introns; therefore, the gene expression profile may reflect the cellular transcriptome and nascent transcription. To allow cross-sample comparisons, we integrated the datasets of all four samples for cell type clustering (Becht et al., 2019; Stuart et al., 2019). The cell type identity was assigned based on the top differentially expressed genes. Eight clusters (designated 0-7) were identified based on the expression of different sets of marker genes (Figures 3D and S3). Among them, clusters 0 and 1 were the most abundant

populations of naive AT2 cells and infected non-proliferative AT2 (tdTomato-GFP+) cells, accounting for more than 26% of all AT2 (GFP+) cells. In contrast, they were reduced to approximately 13% in infected proliferative AT2 (tdTomato + GFP+) cells (Figure 3E). We identified cluster 2 as the most dynamic AT2 cell population among the four samples. Cluster 2 was enriched in infected proliferative AT2 cells, accounting for 58.8% of AT2 cells, but it was greatly reduced to less than 17% in infected non-proliferative AT2 cells and the naive samples (Figure 3E). Cluster 3 accounted for 10-12% of all AT2 cells in all four samples (Figure 3E). Clusters 4 to 7 comprised less than 2% of all AT2 cells in all four samples (Figures 3E and S3A). Therefore, scRNA-seq revealed that cluster 2 was a dynamic AT2 cell population associated with regenerating lungs.

Proliferative AT2 (cluster 2) cell population expands after SpT4 infection-induced injury
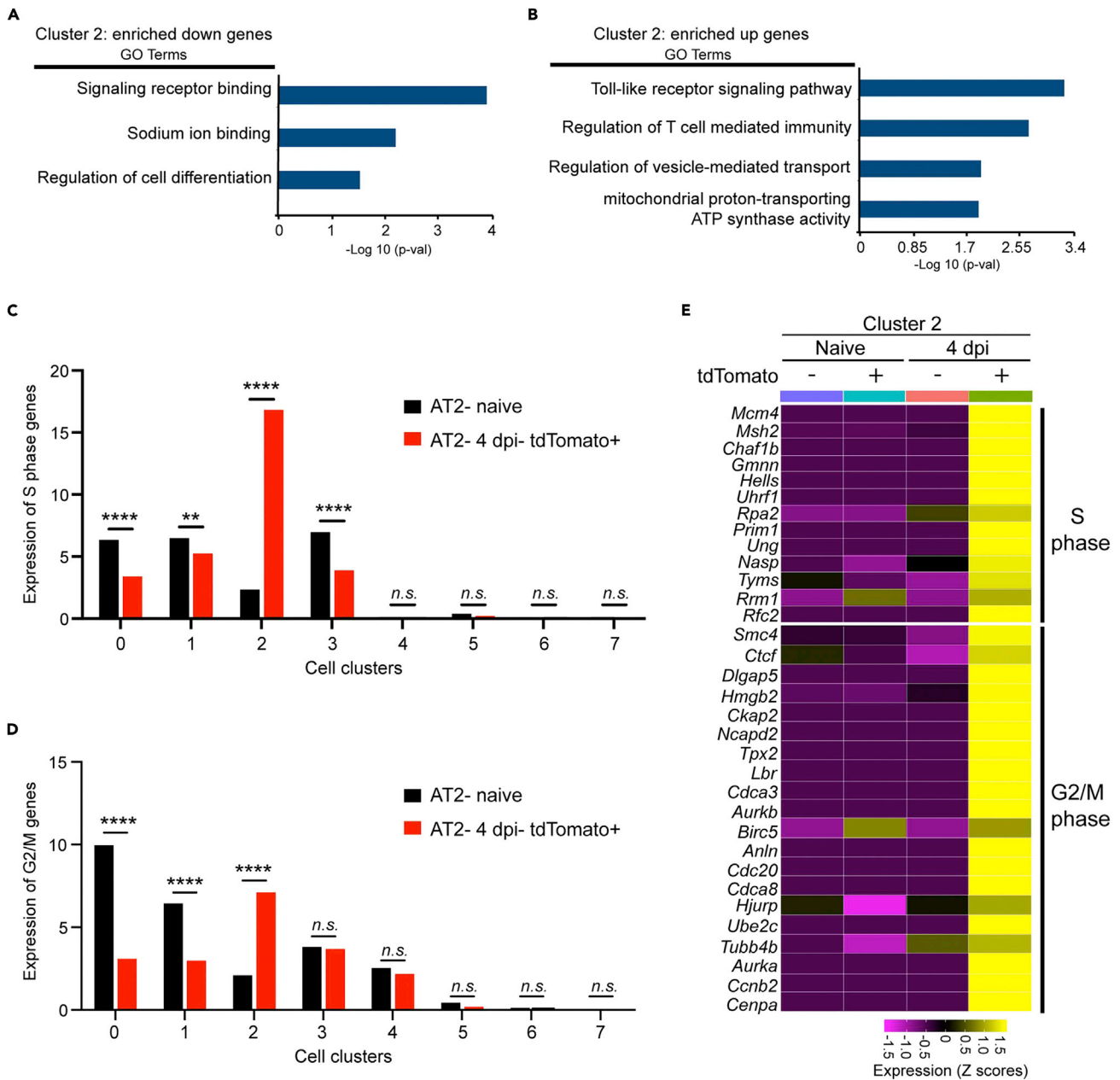
Compared with other AT2 cell populations, cluster 2 cells expressed lower levels of genes associated with signaling receptor binding, sodium ion binding, and regulation of cell differentiation (Figure 4A and Table S1). Cluster 2 cells were significantly enriched for the expression of genes related to Toll-like receptor signaling pathway and regulation of T cell-mediated immunity, suggesting a unique immune state (Figures 4B and Table S1). Cluster 2 cells also expressed high levels of markers associated with vesicle-mediated transporter activity and mitochondrial proton-transporting ATP synthase activity. This suggests that cluster 2 cells may have higher energy production.

As AT2 cell proliferation is a prerequisite for lung alveolar epithelial regeneration, we next assessed the proliferative activity of individual AT2 cell populations using a method based on the proportional expression of genes associated with the S or G2/M cell cycle (Kowalczyk et al., 2015). Analysis of total AT2 cells in infected and naive samples revealed increased AT2 cells mapped to the cycling S phase in proliferative AT2 cells at 4 dpi compared to non-proliferative AT2 cells at 4 dpi and naive AT2 cells (Figure S4A). To determine which population contributed to the increase of S phase AT2 cells following injury, we plotted the fraction of S phase cells in each AT2 population in proliferative AT2 (tdTomato+) cells at 4 dpi compared to naive samples. This analysis showed that only the cluster 2 population had a significant increase in the fraction of S phase cells after injury (Figure 4C). Furthermore, we plotted the fraction of G2/M phase cells in each AT2 population and found only the cluster 2 cells had a significant increase in the fraction of G2/M phase cells after injury (Figure 4D). Additionally, cell-cycle genes associated with the S phase and G2/M phase were strongly activated in cluster 2 cells in proliferative AT2 cells at 4 dpi (Figure 4E). These results suggest a proliferative phenotype of cluster 2 cells after SpT4 infection-induced injury. Although the cluster 0 population contained a high proportion of G2/M cells, unlike cluster 2, cluster 0 cells did not become more proliferative after injury (Figures 4D and S4B). Together, these findings indicate that cluster 2 cells are enriched in regenerative lung alveolar epithelium and enter the cell cycle within 4 days of injury.

Proliferative AT2 (cluster 2) cells are characterized by a defined transcriptional response after injury

To understand the injury response of cluster 2 cells that underlies their proliferative phenotype during alveolar epithelial regeneration, we compared their transcriptomes at four dpi and naïve AT2 cells (Figure 5A). We divided the differentially regulated genes into two groups by their temporal regulation (Figures 5B and Table S2). Genes down-regulated in proliferative cluster 2 (tdTomato+) cells at 4 dpi were associated with Gene Ontology (GO) terms related to phospholipid and cellular lipid metabolic processes and ubiquitin homeostasis (Figure 5B). Genes that showed acute up-regulation were associated with ribosome biogenesis, mitochondrial proton-transporting ATP synthase complex biogenesis, and oxidative phosphorylation. These results suggest altered cellular metabolism in proliferative cluster 2 cells, which may be a prerequisite for cell cycle re-entry (Nakada et al., 2017; Puente et al., 2014). Notably, the activated genes in the proliferative cluster 2 cells after injury were highly correlated with GO terms related to cell cycle regulation, further confirming the active proliferation of cluster 2 cells after injury (Figure 5B). Therefore, after injury induced by SpT4 infection, the transcriptional response of cluster 2 cells involved a reduction in fatty acid biosynthesis and cholesterol metabolism and an increase in ribosome biogenesis, followed by enhanced activation of cell cycle processes.

As it has been shown that the dedifferentiation of adult mature cells is related to the characteristics of progenitor cells (Chang-Panesso and Humphreys, 2017), we examined gene expression associated with immature AT2 cells. Proliferative cluster 2 cells in the injured lungs showed similar expression of most immature AT2 cell markers, including Sox9, Id2, Sox2, Foxp1, Etv5, Wnt7b, Wnt5a, Dkk1, Bmp4, Notch1, Foxa1, Spry2, Thbs1 (De Langhe et al., 2005; Herriges et al., 2012; Eblaghie et al., 2006; Gontan et al., 2008;

Figure 4. Cluster 2 is enriched in the regenerative lungs and becomes proliferative after SpT4 infection-induced injury

(A) Down-regulated genes enriched in cluster 2 populations compared with other cell clusters were analyzed and top statistically enriched Gene Oncology (GO) are plotted by p value.
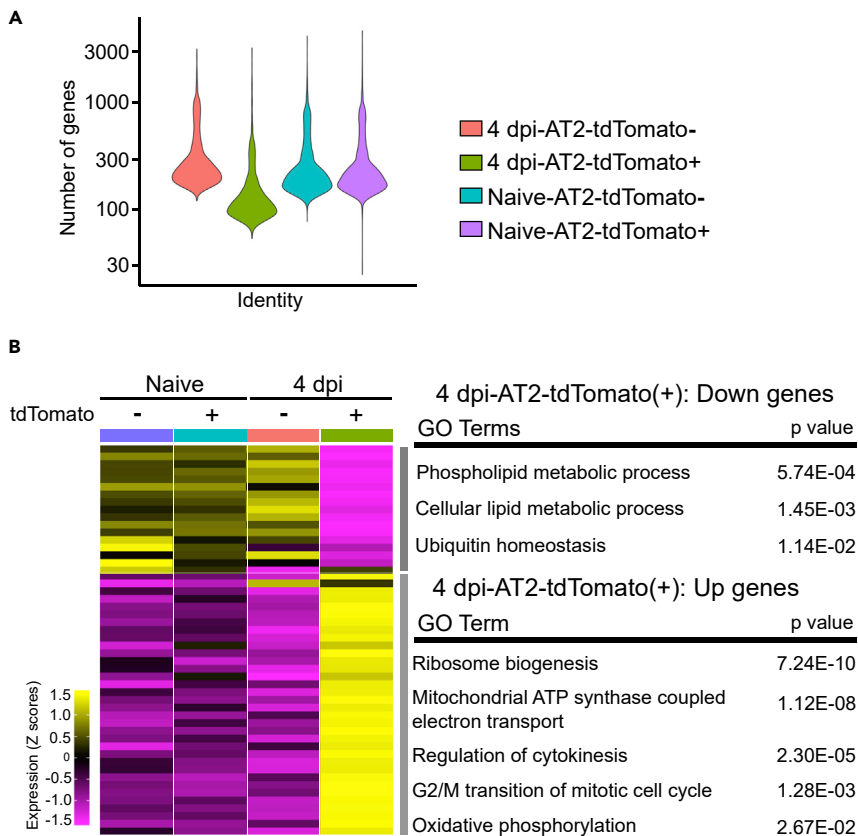
(B) Top GO terms for genes up-regulated in cluster 2 populations compared with other cell clusters are shown.

(C) Percentage of AT2 cells mapped to the S cell-cycle phase in all eight cell clusters from proliferative AT2 (tdTomato+) cells at 4 dpi or naive AT2 (tdTomato- and tdTomato+) cells. **p < 0.01; ****p < 0.0001 (chi-square test).

(D) Percentage of AT2 cells mapped to the G2/M cell-cycle phase in all eight cell clusters. ****p < 0.0001 (chi-square test).

(E) Heatmap showing the relative expression of S phase and G2/M genes in cluster 2 cells from naive AT2 cells and AT2 cells at 4 days after SpT4 infection (4 dpi).

Li et al., 2002; Liu et al., 2003; Liu and Hogan, 2002; Mailleux et al., 2001; Metzger et al., 2007; Perl et al., 2005; Post et al., 2000; Rawlins, 2008; Rawlins et al., 2009; Shu et al., 2002, 2007; Wan et al., 2005) (Figure S4C). In contrast, the expression of immature AT2 cell markers, *Foxp2*, *Elf5*, and *Shh*, was increased in proliferative cluster 2 cells from injured lungs (Figure S4C). This indicates that cluster 2 cells exhibited

A

B

4 dpi-AT2-tdTomato(+): Down genes	
GO Terms	p value
Phospholipid metabolic process	5.74E-04
Cellular lipid metabolic process	1.45E-03
Ubiquitin homeostasis	1.14E-02

| 4 dpi-AT2-tdTomato(+): Up genes	
GO Term	p value
Ribosome biogenesis	7.24E-10
Mitochondrial ATP synthase coupled electron transport	1.12E-08
Regulation of cytokinesis	2.30E-05
G2/M transition of mitotic cell cycle	1.28E-03
Oxidative phosphorylation	2.67E-02

Figure 5. Regenerative response of cluster 2 cells following injury

(A) Violin plots showing the number of detected genes of cluster 2 cells among four samples. dpi: days post-infection.
(B) Hierarchical clustering of differentially expressed genes in cluster 2 cells across samples identified two groups of genes that showed dynamic regulation in response to SpT4 infection-induced lung injury. Left, heatmap of gene expression in Z scores; right, top GO terms enriched for genes in Z scores.

a regenerative response without the need for complete dedifferentiation into an intermediary embryonic-like step at 4 dpi. In addition, Axin2+ AT2 cells have been identified as alveolar progenitor cells (Frank et al., 2016; Nabhan et al., 2018). In this work, we didn't observe significantly higher levels of *Axin2* as well as other *Wnt* genes in cluster 2 cells from injured lungs than those from naive lungs (Figure S4D). This result suggests that cluster 2 cells may represent a distinct AT2 subpopulation that has alveolar progenitor cell activity. Furthermore, Il1r has been suggested to mark a subset of AT2 cells associated with progenitor cell function (Choi et al., 2020). We examined *Il1r1* expression in 8 clusters and four samples (Figure S4E). Among the eight clusters from naive AT2 cells, cluster 1 showed the highest *Il1r1* expression. However, this expression was dramatically decreased in proliferating AT2 cells at 4 dpi. Cluster 5 showed the upregulation of *Il1r1* in proliferating AT2 cells at 4 dpi. However, cluster 5 comprised only about 1.68% of proliferating AT2 cells at 4 dpi. Cluster 3 showed the upregulation of *Il1r1* in non-proliferating AT2 cells at 4 dpi. These data suggest that *Il1r1*-expressing AT2 cells do not play a major role in AT2 cell proliferation during SpT4-infection-induced lung injury and repair.

To delineate the gene program underlying the proliferative phenotype of cluster 2 cells, we next used HOMER 2 to perform motif enrichment analysis in the promoter regions of the up-regulated genes (±5 kb from transcription start sites). The top enriched transcription factor (TF) binding motifs were the ATTAACACCT motif that can be recognized by the EOMES TF, the GTCATGCHTGRCTGS motif that can be recognized by PAX8 TF, the thyroid hormone receptor alpha (THRA) binding motif, and activating transcription factor 3 (ATF3) binding motif, and BTB domain and CNC homolog, basic leucine zipper transcription factor 2 (BACH2) binding motif (Figure 6A). To identify specific TFs that may be related to these motifs, we searched for TFs that were also up-regulated after injury. This analysis showed *Atf3* and *Thra*

A

	p value
ATF3	1E-8
THRA	1E-8
BACH2	1E-8
EOMES	1E-8
PAX8	1E-8

B

C

D

E
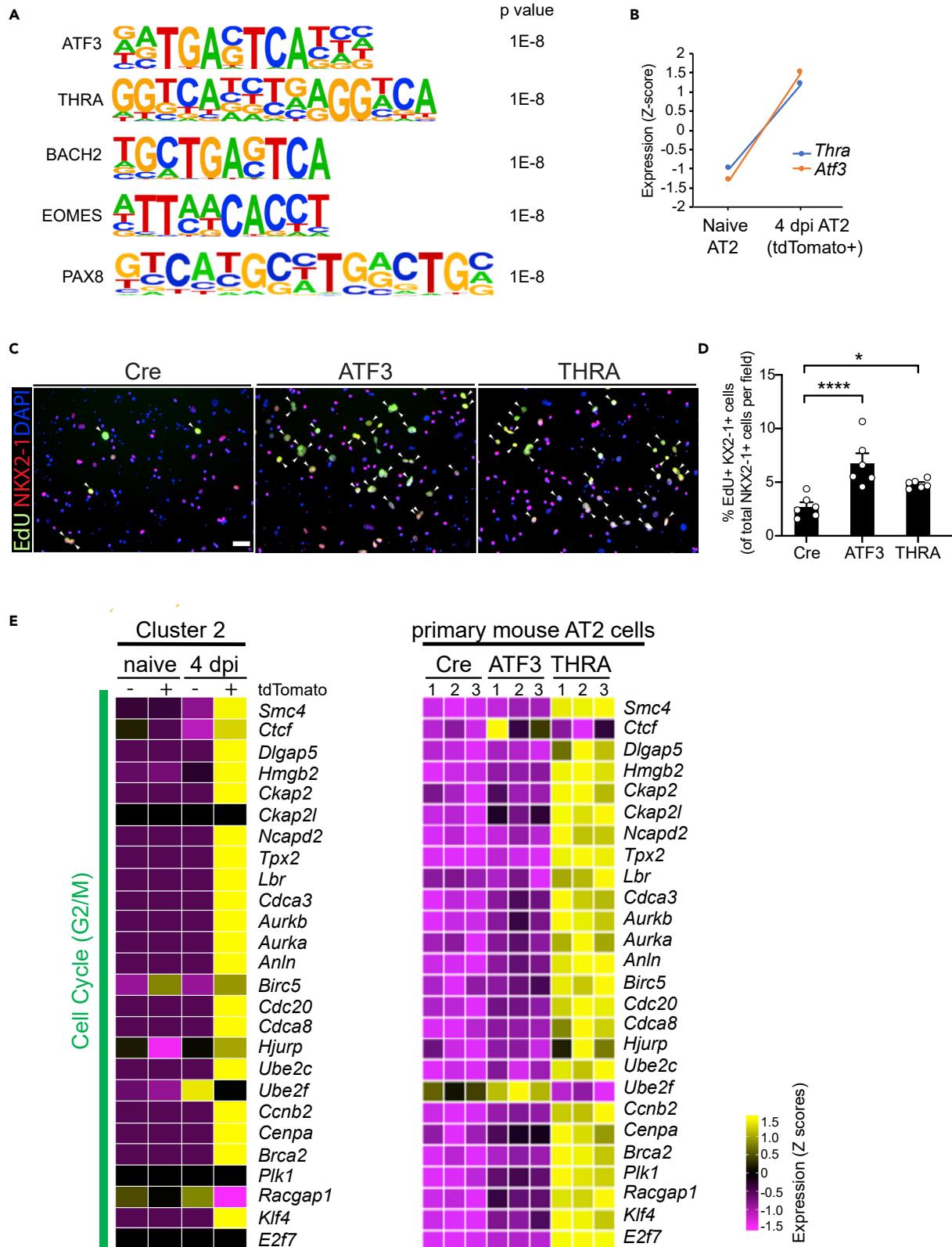
Figure 6. Transcriptional response in cluster 2 cells after injury

(A) Predicted upstream transcriptional factors of cluster 2 proliferative injury response.

(B) Relative expression of *Atf3* and *Thra* in cluster 2 cells from naive AT2 cells and proliferative AT2 (tdTomato+) cells 4 days after infection (4 dpi).

(C) Representative immunostaining of cultured primary mouse AT2 cells showing AT2 cells in DNA synthesis-phase as detected using Click-iT EdU Alexa Fluor (green) and co-immunostaining with antibody against NKX2-1 (red) to detect AT2 cells. Cell nuclear was stained with DAPI (blue). Arrows point to regions double-positive for NKX2-1 and EdU. Scale bar: 50 μm.

(D) Quantification of EdU + NKX2-1+ cells as percentage of total NKX2-1+ cells analyzed (mean ± SEM). *p < 0.05; ****p < 0.0001 (one-way ANOVA).

(E) Heatmap showing expression of selected G2/M cell cycle genes in cluster 2 cells and primary mouse AT2 cells. Z scores of averaged normalized expression values of each gene in cluster 2 cells among four samples from scRNA-seq analysis (left). Z scores of RPKM of each gene in three replicates of mouse primary AT2 cells expressing Ad-Cre, Ad-ATF3, or Ad-THRA from bulk RNA-seq analysis (right).

were up-regulated in cluster 2 cells after injury (Figures 6B and S5A). In addition, immunofluorescence staining for ATF3 and THRA on sectioned lung tissues showed that, compared with naive lungs, SpT4-infected lungs exhibited higher percentage of lineage-labeled AT2 cells (GFP+) that are either ATF3+ or THRA+ (Figures S5B and 5C). This suggests that ATF3 and THRA TFs may act as upstream regulators to drive AT2 cell proliferation after injury.

ATF3 and THRA function as upstream regulators to drive AT2 cell proliferation in response to injury

To determine the functions of ATF3 and THRA, we overexpressed them individually in primary mouse AT2 cells using adenoviruses (Ad) and assessed their ability to promote cell proliferation as measured by EdU incorporation and Ki67 immunostaining. Proliferative AT2 cells were identified by nuclear NKX2-1 staining colocalized with EdU or Ki67. Overexpression of ATF3 or THRA significantly increased the number of EdU + NKX2-1+ and Ki67 + NKX2-1+ cells compared with control (Ad-Cre) (Figures 6C, 6D, and S5D). Additionally, qPCR analysis showed that genes involved in the G2/M phase, such as *Anln, Aurkb, Plk1, and Birc5* were significantly up-regulated in AT2 cells treated with Ad-ATF3 or Ad-THRA compared to those treated with Ad-Cre (Figure S5E). In contrast, overexpression of ATF3 or THRA led to the down-regulation of genes related to programmed cell death (Figure S5F).

To understand the mechanism by which ATF3 and THRA promote the proliferation of AT2 cells, we performed the RNA-seq analysis on AT2 cells overexpressing Cre (control), ATF3, or THRA. Genes specifically upregulated in response to ATF3 overexpression were related to the extracellular matrix organization, actin cytoskeletal organization, and cell junction organization (Figures S5G and S5H). Genes specifically up-regulated by THRA were related to ribosome biogenesis and mitotic cell cycle processes (Figure S5I). In addition, we identified genes upregulated by both ATF3 and THRA, which were related to cell cycle G1/S phase and G2/M phase transition and negative regulation of apoptotic process (Figure S5J). Furthermore, we compared the genes upregulated in response to overexpression of ATF3 or THRA with genes enriched in cluster 2 cells in proliferative AT2 cells after injury (4 dpi). This analysis showed that the activated genes related to the G2/M phase in cluster 2 cells after injury were also markedly upregulated by overexpression of ATF3 or THRA (Figure 6E). Therefore, the overexpression of ATF3 or THRA promotes cell proliferation involved in the injury response of cluster 2 cells.

Overexpression of ATF3 or THRA promoted AT2 cell proliferation and improved lung function after SpT4-induced injury

To examine whether overexpression of ATF3 or THRA could enhance lung repair in response to acute injury, we used adeno-associated virus 6 (AAV6) vector that expressed ATF3-GFP or THRA or GFP (control) and delivered them intratracheally on adult mice. Mouse lungs treated with AAV6-GFP or AAV6-ATF3-GFP exhibited GFP staining in AT2 (Pro-SPC+) cells 48 h after treatment (Figure S6A). In addition, AT2 cells were purified and analyzed for gene expression by qPCR. Mice treated with AAV6-ATF3-GFP or AAV6-THRA showed more than 3 times higher *Atf3* or *Thra* mRNA expression compared with control mice that received AAV6-GFP (Figure S6B). Overexpression of ATF3 or THRA in mouse lungs was sufficient to induce G2/M gene expression in AT2 cells, as AT2 cells treated with AAV6-ATF3 or AAV6-THRA showed increased expression of G2/M genes (*Aurkb, Birc5, Plk1*) compared to AAV6-GFP treatment (Figure S6C). In contrast, overexpression of ATF3 or THRA resulted in a decrease in the expression of the cell cycle suppressor gene (*P27*) (Figure S6C). Furthermore, we analyzed AT2 cell proliferation by EdU labeling assay. Mice treated with

AAV6-ATF3 or AAV6-THRA showed a significantly increased number of EdU + AT2 (pro-SPC+) cells compared with mice treated with AAV6-GFP (Figure S6D).

Next, we performed SpT4 infection on mice and treated them intratracheally with AAV6-ATF3 or AAV6-THRA or AAV6-GFP at 6 dpi (Figure 7A). Forty-eight hours after treatment (8 dpi), we observed that the number of EdU + AT2 (pro-SPC+) cells in the lungs of mice treated with AAV6-ATF3 or AAV6-THRA was significantly higher than that of mice treated with AAV6-GFP (Figure 7B). This indicated that the AT2 cell cycle activity of animals treated with AAV6-ATF3 or AAV6-THRA was greatly increased. Apoptosis in lungs treated with AAV6-ATF3 or AAV6-THRA was not affected, as the number of apoptotic cells (TUNEL+) was equivalent to that of mouse lungs treated with AAV6-GFP (Figure S6E). The functional assessment of the animals 14 days after infection (14 dpi) showed that AAV6-ATF3 or AAV6-THRA treatment reduced SpT4 infection-induced lung compliance increase and forced expiratory volume and forced vital capacity ratio (FEV0.05/FVC) reductions (Figure 7C). The level of aberrantly enlarged air space caused by SpT4 infection was significantly reduced by AAV6-ATF3 or AAV6-THRA treatment, as quantified using a mean linear intercept (MLI) method (Liu et al., 2017) (Figure S6F). Moreover, the level of lung fibrotic lesion formation induced by SpT4 infection was not affected by AAV6-ATF3 or AAV6-THRA treatment (Figure S6G). To determine the effect of ATF3 and THRA overexpression on the differentiation ability of AT2 cells, we infected adult *SPC^{CreERT2}*; *Rosa26^{tdTomato}* mice with SpT4 and delivered AAV6-ATF3 or AAV6-THRA or AAV6-GFP at 6 dpi, and analyzed the differentiation of AT2 cells into AT1 cells at 14 dpi (Figure 7D). We examined AT2-to-AT1 differentiation by quantifying the percentage of RFP + alveolar surface area covered by AT2-derived AT1 cells (RFP + T1α+) and the percentage of RFP and HOPX (AT1 cell marker) double-positive cells on sectioned lungs. Compared with control mice (AAV6-GFP), overexpression of ATF3 or THRA significantly increased the level of the differentiation of AT2 cells into AT1 cells (RFP + T1α+ and RFP + HOPX+) (Figures 7E and S6H). Taken together, these data indicate that overexpression of ATF3 or THRA *in vivo* confers a proliferative and enhanced regenerative effect in lungs after SpT4 infection-induced injury.

DISCUSSION

Our single-cell sequencing and lineage tracing studies have revealed the heterogeneity of AT2 cells in adult lungs. They have different proliferation and differentiation abilities under homeostatic state and regenerative state. But it is still unclear whether there are molecular distinctions between regenerative and non-regenerative AT2 cells. If so, what molecular mechanisms contribute to the AT2 cell regenerative response. In this study, we applied scRNA-seq and lineage tracing to interrogate the transcriptome landscape of adult AT2 cells at a regenerative state. We identify proliferative AT2 (cluster 2) cell populations that elicit differential injury responses after injury. Our results indicate three important features of proliferative AT2 cells in adult lungs. First, among the eight different AT2 cell populations, only the proliferative AT2 (cluster 2) cell population upregulated cell cycle genes and showed an increase in the proportion of cycling AT2 cells after injury. Second, by separately profiling AT2 cells in the G2/M phase from the regenerating lungs, we showed that cycling G2/M AT2 cells were significantly enriched in the cluster 2 population. Third, we observed that cluster 2 population in proliferative AT2 cells at 4 dpi showed a fractional increase compared to naive lungs (from 16% to 58.8%). Our study also identified another proliferative population, cluster 0. Unlike cluster 2, cluster 0 cells did not become more proliferative after injury. Although cluster 0 population may represent another source of proliferative AT2 cells during lung alveolar epithelial regeneration, it is unlikely the only source as cluster 0 is significantly reduced after injury, accounting for only about 13% of the total AT2 cells after injury. Furthermore, cluster 2 cells appear to have high energy production, as evidenced by high levels of genes regulating mitochondrial proton-transporting ATP synthase activity and oxidative phosphorylation. Therefore, cluster 2 cells may adopt a unique metabolic state to cope with the regenerative response.

It has been suggested that the regeneration of adult lung alveolar tissue is associated with the activation of a regenerative program after injury (Kotton and Morrisey, 2014). Here, our scRNA-seq data show that the regenerative and naive AT2 cells in adult lungs displayed defined and distinct injury responses. Our data show that in proliferative AT2 (cluster 2) cells, the down-regulation of phospholipid and cellular lipid metabolism and the up-regulation of ribosome biogenesis precede G2/M cell cycle activation, suggesting that they may be required for injury-induced proliferation. This finding has been reported in other studies, which show that increased ribosome biogenesis and protein synthesis in tumors leads to increased cell proliferation (Cui et al., 2020; Martinez-Outschoorn et al., 2017; Zhou et al., 2015). In addition, cellular plasticity of the regenerative response to injury in organs has been suggested to be associated with the dedifferentiation of adult mature cells, which adopt an embryonic-like phenotype after injury
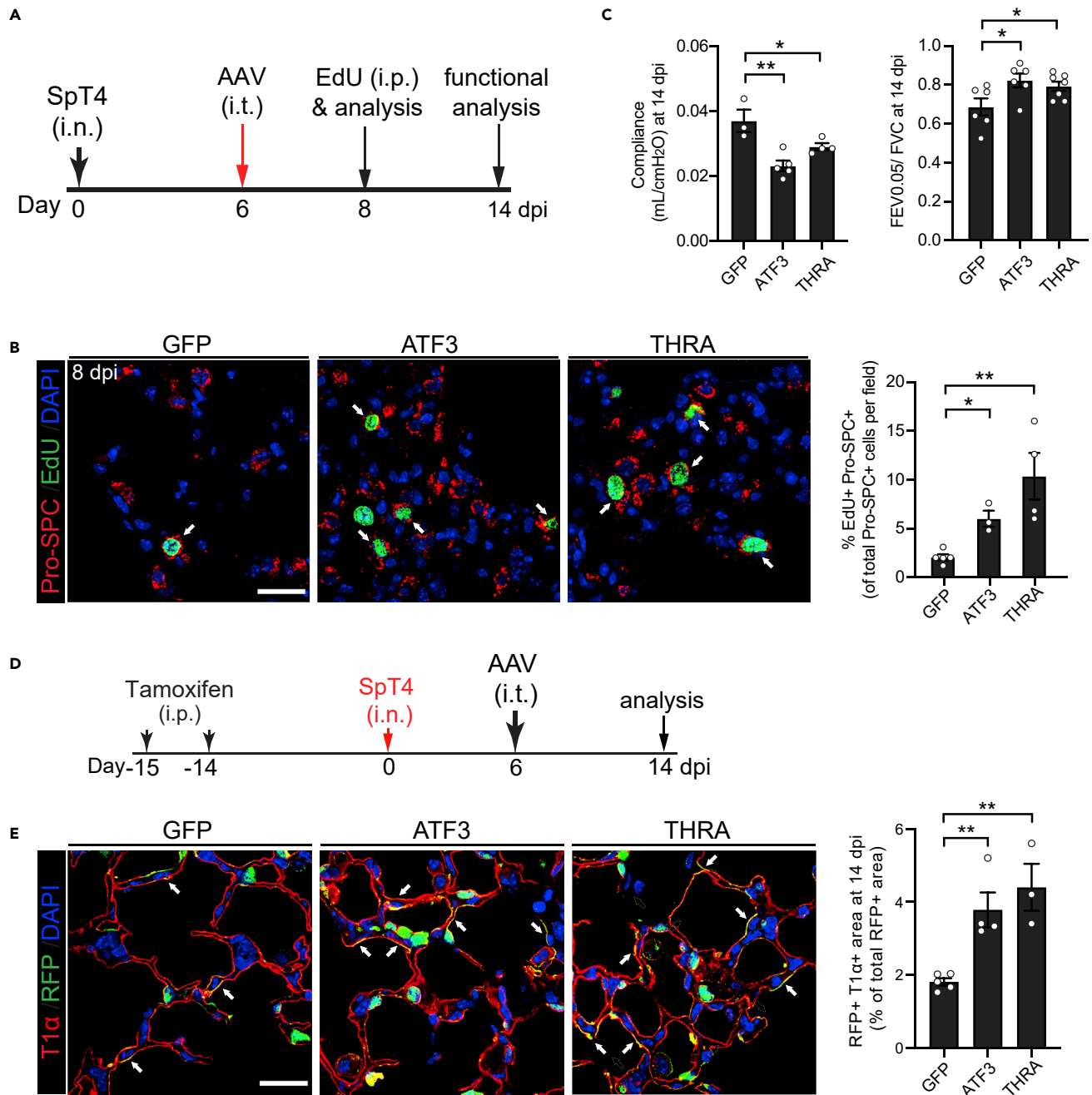
Figure 7. Overexpression of ATF3 or THRA promotes lung repair after injury

(A) Schematic showing the experimental design for AAV6 instillation and time points of sample collections. i.n.: intranasally; i.t.: intratracheally; i.p.: intraperitoneally.

(B) Confocal images of immunostaining of Pro-SPC (red) and EdU (green) on lung sections from mice treated with AAV6-GFP or AAV6-ATF3 or AAV6-THRA at 8 days after SpT4 infection (8 dpi). Cell nuclear was stained with DAPI (blue). Arrows point to regions double-positive for Pro-SPC and EdU. Graph on the right showing a fold change in the percentage of Pro-SPC + EdU+ of total Pro-SPC + cells analyzed.

(C) Compliance and forced expiration extension (FEV) in the first 0.05 s of forced vital capacity (FVC) were recorded using *flexiVent* in mice treated with AAV6-GFP or AAV6-ATF3 or AAV6-THRA at 14 dpi.

(D) Experimental design for studies performed in (E) using $Sftpc^{CreERT2}$; $Rosa26^{tdTomato}$ adult mice.

(E) Confocal images of lung sections at 14 dpi with immunostaining with antibodies to RFP (green) and T1α (red), an AT1 cell marker, to detect the differentiation of lineage-labeled AT2 cells into AT1 cells. Arrows point to regions double-positive for RFP and T1α. Graph on the right showing fold change in the percentage of RFP + T1α+ area of total RFP + area per field using ImageJ. Scale bars: 20 μm in (B, E). Data are presented in (B, C, E) as mean ± SEM *p < 0.05; **p < 0.01. p values were calculated using one-way ANOVA.

(Chang-Panesso and Humphreys, 2017). In our lung epithelial injury model, we did not observe proliferative AT2 (cluster 2) cells express higher levels of markers of immature AT2 cells, including S*ox9, Id2, Sox2, Foxp2, Foxp1, Etv5, Wnt7b, Wnt5a, Dkk1, Bmp4, Notch1, Foxa1, Spry2, Thbs1* (De Langhe et al., 2005; Herriges et al., 2012; Eblaghie et al., 2006; Gontan et al., 2008; Li et al., 2002; Liu et al., 2003; Liu and Hogan, 2002; Mailleux et al., 2001; Metzger et al., 2007; Perl et al., 2005; Post et al., 2000; Rawlins, 2008; Rawlins et al., 2009; Shu et al., 2002, 2007; Wan et al., 2005). This suggests that the regenerative response of proliferative AT2 (cluster 2) cells does not need to dedifferentiate into an intermediary embryonic-like step at 4 dpi. Additionally, Axin2+ AT2 cells have been identified as alveolar progenitor cells, which slowly self-renew at a steady state and become expanded after epithelial injury (Frank et al., 2016; Nabhan et al., 2018). Il1r + has been suggested to mark a subset of AT2 cells associated with progenitor cell function (Choi et al., 2020). Our scRNA-seq data showed that cluster 2 cells do not express higher levels of *Axin2*, other *Wnt* genes, and *Il1r* from injured lungs than those from naive lungs, suggesting that cluster 2 cells may represent a distinct subset of AT2 cells with alveolar progenitor cell activity, at least in this SpT4 infection-induced lung injury model.

The ability of the regenerative lung alveolus to repair the damage through cell proliferation has led to attempts to induce cell cycle re-entry of mature differentiated AT2 cells, including manipulations of microRNAs, Hippo signaling, and KGF signaling (Chang-Panesso and Humphreys, 2017; Kowalczyk et al., 2015; LaCanna et al., 2019; Tettelin et al., 2001). Our findings demonstrate that two transcription factors, ATF3 and THRA, induced by injury in cluster 2 regenerative AT2 cells, can efficiently induce AT2 cell proliferation *in vitro* and *in vivo*. Intratracheal AAV6 delivery of these two factors promoted alveolar epithelial repair and regeneration and improved lung function after injury.

The effects of ATF3 and THRA on cell proliferation have been demonstrated in multiple organs. ATF3 seems to directly activate cell cycle progression, as evidenced by the upregulation of many cell cycle genes and G2/M-related GO terms. ATF3 is a member of the ATF/cAMP response element-binding (CREB) family, which binds to the cyclic AMP response element in numerous promoters (Deutsch et al., 1988; Montminy and Bilezikjian, 1987). It has been shown to regulate the proliferation of osteoclast precursors (Deutsch et al., 1988) and protect lungs from acute injury by preventing the degradation of NRF2 (Akram et al., 2010; Fukasawa et al., 2016; Shan et al., 2015). It was found that THRA can induce the proliferation of neural cells and regulate the proliferation and differentiation of skeletal muscle myoblasts (Milanesi et al., 2016; Wen et al., 2019). In pancreatic β cells, THRA was found to protect cells from oxidative ER stress (Takahashi et al., 2014). Our RNA-seq data are consistent with these findings, as overexpression of ATF3 or THRA in AT2 cells leads to the upregulation of genes involved in cell proliferation. Together, our results indicate that the endogenous response to injury in regenerative alveolar epithelium can identify factors that can be used to improve lung repair and function. Long-term induction of AT2 proliferation may cause adverse effects. In our study, ATF3 or THRA overexpressing lungs were evaluated 2 weeks after SpT4 infection, and the results showed that alveolar epithelial repair and lung function were improved. Therefore, the expression of ATF3 and THRA provides proliferative benefits for injured lungs.

Limitations of the study

Although our studies showed that proliferative AT2 (cluster 2) cells did not express higher levels of immature AT2 cell and *Wnt* gene markers at 4 dpi, it is possible that altered expression of these genes occurred at earlier time points after injury. Further studies are needed to assess whether proliferative AT2 (cluster 2) cells have an AT2 cell dedifferentiation program or a *Wnt* gene program before 4 dpi. In addition, although we have identified factors that can be used to improve lung repair and function in response to injury caused by SpT4 infection, it is not possible to extrapolate our findings from these experiments to all species or all models of lung injury. In the future, these factors will be applied to other injury models, such as COPD lungs and aging lungs, where AT2 cells have minimal regenerative capacity. These future works may provide new strategies for developing therapies to repair and regenerate lungs.

STAR★METHODS

Detailed methods are provided in the online version of this paper and include the following:

- KEY RESOURCES TABLE
- RESOURCE AVAILABILITY
  - Lead contact

SUPPLEMENTAL INFORMATION

Supplemental information can be found online at https://doi.org/10.1016/j.isci.2022.104843.

AUTHOR CONTRIBUTIONS

M.A. performed the majority of the experiments and participated in writing the article. R.L. performed AT2 cell isolation and cell sorting for single-cell RNA sequencing. Z.L. and J.H. advised on scRNA-seq. Y.F.T. performed bulk RNA seq and data analysis. X.Y. and W.S. performed scRNA-seq analysis. Y. T. supervised all experiments and wrote the article.

DECLARATION OF INTERESTS

The authors declare no competing interests.

REFERENCES

Akram, A., Han, B., Masoom, H., Peng, C., Lam, E., Litvack, M.L., Bai, X., Shan, Y., Hai, T., Batt, J., et al. (2010). Activating transcription factor 3 confers protection against ventilator-induced lung injury. Am. J. Respir. Crit. Care Med. *182*, 489–500. https://doi.org/10.1164/rccm.200906-0925OC.

Barkauskas, C.E., Cronce, M.J., Rackley, C.R., Bowie, E.J., Keene, D.R., Stripp, B.R., Randell, S.H., Noble, P.W., and Hogan, B.L.M. (2013). Type 2 alveolar cells are stem cells in adult lung. J. Clin. Invest. *123*, 3025–3036. PMID: 23921127. https://doi.org/10.1172/JCI68782.

Becht, E., McInnes, L., Healy, J., Dutertre, C.A., Kwok, I.W.H., Ng, L.G., Ginhoux, F., and Newell, E.W. (2019). Dimensionality reduction for visualizing single-cell data using UMAP. Nat.

Biotechnol. *37*, 38–44. https://doi.org/10.1038/nbt.4314.

Chang-Panesso, M., and Humphreys, B.D. (2017). Cellular plasticity in kidney injury and repair. Nat. Rev. Nephrol. *13*, 39–46. https://doi.org/10.1038/nrneph.

Choi, J., Park, J.E., Tsagkogeorga, G., Yanagita, M., Koo, B.K., Han, N., and Lee, J.H. (2020). Inflammatory Signals induce AT2 cell-derived damage-associated transient progenitors that mediate alveolar regeneration. Cell Stem Cell *27*, 366–382.e7. https://doi.org/10.1016/j.stem.2020.06.020.

Clevers, H. (2015). STEM CELLS. What is an adult stem cell? Science *350*, 1319–1320. https://doi.org/10.1126/science.aad7016.

Cui, M., Wang, Z., Chen, K., Shah, A.M., Tan, W., Duan, L., Sanchez-Ortiz, E., Li, H., Xu, L., Liu, N., et al. (2020). Dynamic transcriptional responses to injury of regenerative and non-regenerative Cardiomyocytes revealed by single-nucleus RNA sequencing. Dev. Cell *53*, 102–116.e8. https://doi.org/10.1016/j.devcel.2020.02.019.

de Hoon, M.J.L., Imoto, S., Nolan, J., and Miyano, S. (2004). Open source clustering software. Bioinformatics *20*, 1453–1454. https://doi.org/10.1093/bioinformatics/bth078.

De Langhe, S.P., Sala, F.G., Del Moral, P.M., Fairbanks, T.J., Yamada, K.M., Warburton, D., Burns, R.C., and Bellusci, S. (2005). Dickkopf-1 (dkk1) reveals that fibronectin is a major target of

Wnt signaling in branching morphogenesis of the mouse embryonic lung. Dev. Biol. *277*, 316–331. https://doi.org/10.1016/j.ydbio.2004.09.023.

Deutsch, P.J., Hoeffler, J.P., Jameson, J.L., Lin, J.C., and Habener, J.F. (1988). Structural determinants for transcriptional activation by cAMP-responsive DNA elements. J. Biol. Chem. *263*, 18466–18472. PMID: 2848037.

Eblaghie, M.C., Reedy, M., Oliver, T., Mishina, Y., and Hogan, B.L.M. (2006). Evidence that autocrine signaling through bmpr1a regulates the proliferation, survival and morphogenetic behavior of distal lung epithelial cells. Dev. Biol. *291*, 67–82. https://doi.org/10.1016/j.ydbio.2005.12.006.

Frank, D.B., Peng, T., Zepp, J.A., Snitow, M., Vincent, T.L., Penkala, I.J., Cui, Z., Herriges, M.J., Morley, M.P., Zhou, S., et al. (2016). Emergence of a wave of Wnt signaling that regulates lung alveologenesis by Controlling epithelial self-renewal and differentiation. Cell Rep. *17*, 2312–2325. https://doi.org/10.1016/j.celrep.2016.11.001.

Fukasawa, K., Park, G., Iezaki, T., Horie, T., Kanayama, T., Ozaki, K., Onishi, Y., Takahata, Y., Yoneda, Y., Takarada, T., et al. (2016). ATF3 controls proliferation of osteoclast precursor and bone remodeling. Sci. Rep. 6, 30918. https://doi.org/10.1038/srep30918.

Gontan, C., de Munck, A., Vermeij, M., Grosveld, F., Tibboel, D., and Rottier, R. (2008). Sox2 is important for two crucial processes in lung development: branching morphogenesis and epithelial cell differentiation. Dev. Biol. *317*, 296–309. https://doi.org/10.1016/j.ydbio.2008.02.035.

Herriges, J.C., Yi, L., Hines, E.A., Harvey, J.F., Xu, G., Gray, P.A., Ma, Q., and Sun, X. (2012). Genome-scale study of transcription factor expression in the branching mouse lung. Dev. Dyn. *241*, 1432–1453. https://doi.org/10.1002/dvdy.23823.

Hogan, B.L.M., Barkauskas, C.E., Chapman, H.A., Epstein, J.A., Jain, R., Hsia, C.C.W., Niklason, L., Calle, E., Le, A., Randell, S.H., et al. (2014). Repair and regeneration of the respiratory system: complexity, plasticity, and mechanisms of lung stem cell function. Cell Stem Cell 15, 123–138. https://doi.org/10.1016/j.stem.2014.07.012.

Hutchins, J.R.A., Toyoda, Y., Hegemann, B., Poser, I., Hériché, J.K., Sykora, M.M., Augsburg, M., Hudecz, O., Buschhorn, B.A., Bulkescher, J., et al. (2010). Systematic analysis of human protein complexes identifies chromosome segregation proteins. Science *328*, 593–599. https://doi.org/10.1126/science.1181348.

Kotton, D.N., and Morrisey, E.E. (2014). Lung regeneration: mechanisms, applications and emerging stem cell populations. Nat. Med. *20*, 822–832. https://doi.org/10.1038/nm.3642.

Kowalczyk, M.S., Tirosh, I., Heckl, D., Rao, T.N., Dixit, A., Haas, B.J., Schneider, R.K., Wagers, A.J., Ebert, B.L., and Regev, A. (2015). Single-cell RNA-seq reveals changes in cell cycle and differentiation programs upon aging of hematopoietic stem cells. Genome Res. *25*, 1860–1872. https://doi.org/10.1101/gr.192237.115.

Kretzschmar, K., Post, Y., Bannier-Hélaouët, M., Mattiotti, A., Drost, J., Basak, O., Li, V.S.W., van den Born, M., Gunst, Q.D., Versteeg, D., et al. (2018). Profiling proliferative cells and their progeny in damaged murine hearts. Proc. Natl. Acad. Sci. USA 115, E12245–E12254. https://doi.org/10.1073/pnas.1805829115.

LaCanna, R., Liccardo, D., Zhang, P., Tragesser, L., Wang, Y., Cao, T., Chapman, H.A., Morrisey, E.E., Shen, H., Koch, W.J., et al. (2019). Yap/Taz regulate alveolar regeneration and resolution of lung inflammation. J. Clin. Invest. *129*, 2107–2122. https://doi.org/10.1172/JCI125014.

Li, C., Xiao, J., Hormi, K., Borok, Z., and Minoo, P. (2002). Wnt5a participates in distal lung morphogenesis. Dev. Biol. *248*, 68–81. https://doi.org/10.1006/dbio.2002.0729.

Liu, Y., and Hogan, B.L.M. (2002). Differential gene expression in the distal tip endoderm of the embryonic mouse lung. Gene Expr. Patterns *2*, 229–233. https://doi.org/10.1016/s1567-133x(02)00057-1.

Liu, Y., Jiang, H., Crawford, H.C., and Hogan, B.L.M. (2003). Role for ETS domain transcription factors Pea3/Erm in mouse lung development. Dev. Biol. *261*, 10–24. https://doi.org/10.1016/s0012-1606(03)00359-2.

Liu, Z., Fu, S., and Tang, N. (2017). A Standardized method for measuring internal lung surface area via mouse pneumonectomy and prosthesis implantation. J. Vis. Exp. *26*, 56114. https://doi.org/10.3791/56114.

Mailleux, A.A., Tefft, D., Ndiaye, D., Itoh, N., Thiery, J.P., Warburton, D., and Bellusci, S. (2001). Evidence that sprouty2 functions as an inhibitor of mouse embryonic lung growth and morphogenesis. Mech. Dev. *102*, 81–94. https://doi.org/10.1016/s0925-4773(01)00286-6.

Martinez-Outschoorn, U.E., Peiris-Pagés, M., Pestell, R.G., Sotgia, F., and Lisanti, M.P. (2017). Cancer metabolism: a therapeutic perspective. Nat. Rev. Clin. Oncol. *14*, 11–31. https://doi.org/10.1038/nrclinonc.2016.60.

Metzger, D.E., Xu, Y., and Shannon, J.M. (2007). Elf5 is an epithelium-specific, fibroblast growth factor-sensitive transcription factor in the embryonic lung. Dev. Dyn. *236*, 1175–1192. https://doi.org/10.1002/dvdy.21133.

Milanesi, A., Lee, J.W., Kim, N.H., Liu, Y.Y., Yang, A., Sedrakyan, S., Kahng, A., Cervantes, V., Tripuraneni, N., Cheng, S.Y., et al. (2016). Thyroid hormone receptor α plays an essential role in male skeletal muscle myoblast proliferation, differentiation, and response to injury. Endocrinology *157*, 4–15. https://doi.org/10.1210/en.2015-1443.

Montminy, M.R., and Bilezikjian, L.M. (1987). Binding of a nuclear protein to the cyclic-AMP response element of the somatostatin gene. Nature *328*, 175–178. https://doi.org/10.1038/328175a0.

Nabhan, A.N., Brownfield, D.G., Harbury, P.B., Krasnow, M.A., and Desai, T.J. (2018). Single-cell Wnt signaling niches maintain stemness of alveolar type 2 cells. Science *359*, 1118–1123. https://doi.org/10.1126/science.aam6603.

Nakada, Y., Canseco, D.C., Thet, S., Abdisalaam, S., Asaithamby, A., Santos, C.X., Shah, A.M., Zhang, H., Faber, J.E., Kinter, M.T., et al. (2017). Hypoxia induces heart regeneration in adult mice. Nature *541*, 222–227. https://doi.org/10.1038/nature20173.

Navarro, S., and Driscoll, B. (2017). Regeneration of the aging lung: a mini-review. Gerontology *63*, 270–280. https://doi.org/10.1159/000451081.

Perl, A.K.T., Kist, R., Shan, Z., Scherer, G., and Whitsett, J.A. (2005). Normal lung development and function after Sox9 inactivation in the respiratory epithelium. Genesis *41*, 23–32.

Post, L.C., Ternet, M., and Hogan, B.L. (2000). Notch/delta expression in the developing mouse lung. Mech. Dev. *98*, 95–98. https://doi.org/10.1016/s0925-4773(00)00432-9.

Puente, B.N., Kimura, W., Muralidhar, S.A., Moon, J., Amatruda, J.F., Phelps, K.L., Grinsfelder, D., Rothermel, B.A., Chen, R., Garcia, J.A., et al. (2014). The oxygen-rich postnatal environment induces cardiomyocyte cell-cycle arrest through DNA damage response. Cell *157*, 565–579. https://doi.org/10.1016/j.cell.2014.03.032.

Rawlins, E.L. (2008). Lung epithelial progenitor cells: lessons from development. Proc. Am. Thorac. Soc. 5, 675–681. https://doi.org/10.1513/pats.200801-006AW.

Rawlins, E.L., Clark, C.P., Xue, Y., and Hogan, B.L.M. (2009). The Id2+ distal tip lung epithelium contains individual multipotent embryonic progenitor cells. Development *136*, 3741–3745. https://doi.org/10.1242/dev.037317.

Shan, Y., Akram, A., Amatullah, H., Zhou, D.Y., Gali, P.L., Maron-Gutierrez, T., González-López, A., Zhou, L., Rocco, P.R.M., Hwang, D., et al. (2015). ATF3 protects pulmonary resident cells from acute and ventilator-induced lung injury by preventing Nrf2 degradation. Antioxid. Redox Signal. *22*, 651–668. https://doi.org/10.1089/ars.2014.5987.

Shu, W., Lu, M.M., Zhang, Y., Tucker, P.W., Zhou, D., and Morrisey, E.E. (2007). Foxp2 and foxp1 cooperatively regulate lung and esophagus development. Development *134*, 1991–2000. https://doi.org/10.1242/dev.02846.

Shu, W., Jiang, Y.Q., Lu, M.M., and Morrisey, E.E. (2002). Wnt7b regulates mesenchymal proliferation and vascular development in the lung. Development *129*, 4831–4842. https://doi.org/10.1242/dev.129.20.4831.

Stuart, T., Butler, A., Hoffman, P., Hafemeister, C., Papalexi, E., Mauck, W.M., 3rd, Hao, Y., Stoeckius, M., Smibert, P., and Satija, R. (2019). Comprehensive integration of single-cell data. Cell *177*, 1888–1902.e21. https://doi.org/10.1016/j.cell.2019.05.031.

Takahashi, K., Furuya, F., Shimura, H., Kaneshige, M., and Kobayashi, T. (2014). Impaired oxidative endoplasmic reticulum stress response caused by deficiency of thyroid hormone receptor α. J. Biol. Chem. *289*, 12485–12493. https://doi.org/10.1074/jbc.M113.544122.

Tettelin, H., Nelson, K.E., Paulsen, I.T., Eisen, J.A., Read, T.D., Peterson, S., Heidelberg, J., DeBoy, R.T., Haft, D.H., Dodson, R.J., et al. (2001). Complete genome sequence of a virulent isolate

of Streptococcus pneumoniae. Science *293*, 498–506. https://doi.org/10.1126/science.1061217.

Vanderbilt, J.N., Gonzalez, R.F., Allen, L., Gillespie, A., Leaffer, D., Dean, W.B., Chapin, C., and Dobbs, L.G. (2015). High-efficiency type II cell-enhanced green fluorescent protein expression facilitates cellular identification, tracking, and isolation. Am. J. Respir. Cell Mol. Biol. *53*, 14–21. https://doi.org/10.1165/rcmb.2014-0348MA.

Wan, H., Dingle, S., Xu, Y., Besnard, V., Kaestner, K.H., Ang, S.L., Wert, S., Stahlman, M.T., and Whitsett, J.A. (2005). Compensatory

roles of Foxa1 and Foxa2 during lung morphogenesis. J. Biol. Chem. *280*, 13809–13816. https://doi.org/10.1074/jbc.M414122200.

Wang, Y., Li, Y., Zhang, P., Baker, S.T., Wolfson, M.R., Weiser, J.N., Tian, Y., and Shen, H. (2019). Regenerative therapy based on miRNA-302 mimics for enhancing host recovery from pneumonia caused by Streptococcus pneumoniae. Proc. Natl. Acad. Sci. USA *116*, 8493–8498. https://doi.org/10.1073/pnas.1818522116.

Wen, L., He, C., Sifuentes, C.J., and Denver, R.J. (2019). Thyroid hormone

receptor alpha is required for thyroid hormone-dependent neural cell proliferation during tadpole metamorphosis. Front. Endocrinol. *10*, 396. https://doi.org/10.3389/fendo.2019.00396.

Whitfield, M.L., George, L.K., Grant, G.D., and Perou, C.M. (2006). Common markers of proliferation. Nat. Rev. Cancer 6, 99–106. https://doi.org/10.1038/nrc1802.

Zhou, X., Liao, W.J., Liao, J.M., Liao, P., and Lu, H. (2015). Ribosomal proteins: functions beyond the ribosome. J. Mol. Cell Biol. *7*, 92–104. https://doi.org/10.1093/jmcb/mjv014.

STAR★METHODS

KEY RESOURCES TABLE

REAGENT or RESOURCE	SOURCE	IDENTIFIER
Antibodies		
Rabbit polyclonal anti-mouse proSP-C (used at 1:200)	Millipore	AB3786
Hamster monoclonal (8.1.1) anti-mouse T1a (used 1:200)	Developmental Studies Hybridoma Bank, University of Iowa	8.1.1-c
Goat polyclonal anti-GFP (used at 1:200)	Abcam	ab6673
Chicken polyclonal anti-GFP (used at 1:250)	Aves Labs	GFP1020
Rabbit polyclonal anti-RFP (used at 1:250)	Rockland	600-401-379
Rabbit monoclonal (SP6) anti-mouse Ki67 (used at 1:100)	Abcam	ab16667
Mouse monoclonal (8D5) anti-mouse Ki67 (used at 1:100)	Cell Signaling Technology	9449
Rabbit polyclonal anti-ATF3 (used at 1:50)	ABclonal	A13469
Rabbit polyclonal anti-THRA (used at 1:25)	Invitrogen	PA1-211A
Rabbit monoclonal anti-mouse TTF-1/Nkx2-1 (used at 1:250)	Abcam	ab76013
mouse monoclonal anti-HOP (HOPX, used at 1:50)	Santa Cruz	sc-398703
Chicken anti-Goat IgG (H + L) Secondary Antibody, Alexa Fluor 488 (used at 1:500)	Thermo Fisher Scientific	A-21467
Goat anti-Rabbit IgG (H + L) Secondary Antibody, Alexa Fluor 488 (used at 1:500)	Thermo Fisher Scientific	A-11008
Goat anti-Rabbit IgG (H + L) Secondary Antibody, Alexa Fluor 568 (used at 1:500)	Thermo Fisher Scientific	A-11011
Goat anti-Hamster IgG (H + L) Secondary Antibody, Alexa Fluor 568 (used at 1:500)	Thermo Fisher Scientific	A-21112
Goat anti-Mouse IgG (H + L) Secondary Antibody, Alexa Fluor 568 (used at 1:500)	Thermo Fisher Scientific	A-11004
rabbit anti-Chicken IgY (H + L) FITC conjugate	Jackson Immuno Research Lab	303-095-003
Bacterial and virus strains		
Streptococcus pneumoniae stain T4	LaCanna et al.2019	https://doi.org/10.1172/JCI125014
Ad-ATF3	Vector Biolabs	ADV-253206
Ad-THRA	Applied Biological Materials Inc	466670540200
AAV6-ATF3-GFP	Applied Biological Materials Inc	126091040216
AAV6-THRA	Applied Biological Materials Inc	466671040116
Chemicals		
Tamoxifen	Sigma-Aldrich	T5648
EdU (5-ethynyl-20-deoxyuridine)	Thermo Fisher Scientific	E10415
Bovine Serum Albumin	Gemini Biio-Products	700-100P
Dispase (used at 25 U/ml)	BD Biosciences, Corning	354235
DNase I (used at 120 U/ml)	Sigma-Aldrich	DN25
Red Blood Cell Lysis Buffer	Thermo Fisher Scientific	00-4333
LS Columns	Miltenyi Biotec	130-042-401

Continued

REAGENT or RESOURCE	SOURCE	IDENTIFIER
CD45 Microbeads, mouse - lyophilized	Miltenyi Biotec Incorporated	130-097-153
Streptavidin Microbeads	Miltenyi Biotec Incorporated	130-048-101
FcR Blocking Reagent, mouse	Miltenyi Biotec Incorporated	130-092-575
DMEM /F12 Medium	Invitrogen	21041025
Fetal Bovine Serum	Gemini Bio-Prodcuts	100-106
Deposited data		
Raw scRNA-seq	This paper	GSE184405
Raw bulk RNA-seq	This paper	GSE183129
Software and algorithms		
ImageJ (version 1.48)	NIH	https://imagej.nih.gov/ij/
FIJI	open source	https://imagej.net/Fiji/
GraphPad Prism 9.0	GraphPad Software Inc.	http://www.graphpad.com/scientific-software/prism/
ToppGene	ToppGene Suite	https://toppgene.cchmc.org/enrichment.jsp
Cell-cycle analysis	Kowalczyk et al., 2015	https://satijalab.org/seurat/v4.0/cell_cycle_vignette.html

RESOURCE AVAILABILITY

Lead contact

Further information and requests for resources and reagents should be directed to and will be fulfilled by the lead contact, Ying Tian (ying.tian@temple.edu).

Materials availability

The study did not generate new unique reagents.

Data and code availability

- Single-cell RNA-seq data and bulk RNA-seq data have been deposited at GEO and are publicly available as of the date of publication. Accession numbers are listed in the key resources table. Microscopy data reported in this paper will be shared by the lead contact upon request.

- This paper does not report original code.

- Any additional information required to reanalyze the data reported in this paper is available from the lead contact upon request.

EXPERIMENTAL MODEL AND SUBJECT DETAILS

Mice were bred and raised at Temple University mouse facility. Wild-type C57BL/6 (Jackson Laboratories), *Ki67^CreERT2^* (Jackson Laboratories), *Rosa26^tdTomato^* (Jackson Laboratories), *Rosa26^EYFP^* (Jackson Laboratories), *SPC^EGFP^* (Jackson Laboratories), and *Sftpc^CreERT2^* (7) mice were used. All experiments used 6- to 10-week-old mice. Both genders of mice were used and kept on a mixed genetic background. All the animal experiments were carried out by the NIH guidelines (Guide for the care and use of laboratory animals). All experimental procedures involving animals in this study were reviewed and approved by the Institutional Animal Care and Use Committee of Temple University Medical Center.

METHOD DETAILS

Bacterial infection

Bacterial infection was performed using previously described protocols (LaCanna et al., 2019). Briefly, the clinical isolated pneumococcal strain *Streptococcus pneumoniae* stain T4 (SpT4) was grown in tryptic soy agar plus catalase (57 μgP/ml) under microaerophilic conditions for 14–16 hours at 37°C with 5% CO2, then subcultured and grown to an optical density of 0.5. SpT4 was then collected by centrifuging and

resuspended in PBS. Anesthetized mice using ketamine/xylazine mixture were infected intranasally with a dose of approximately 5×10^6 colony-forming units (CFU) in 30 μL of sterile PBS.

Tamoxifen and EdU administration

Tamoxifen (T5648, Sigma) was dissolved in corn oil (C8267, Sigma) to make a 20 mg/mL stock solution. Mice were given via intraperitoneal injection (200 mg/kg) to activate the Cre recombinase. EdU was administered via intraperitoneal injection (50 mg/kg), followed by a chase of 3 hours.

Histology and immunohistochemistry

Lung tissue histology and immunohistochemistry were performed using previously described protocols (LaCanna et al., 2019). Cells cultures were prepared for staining by fixing in 2% paraformaldehyde, permeabilizing in 0.2% Triton-X and blocked using 1% bovine serum albumin. Cell proliferation was measured using Click-iT® EdU (5-ethynyl-2'-deoxyuridine) Alexa Fluor® Imaging Kit (Thermo). Cell apoptosis was measured using *In Situ* Cell Death Detection Kit, TMR red from Roche. Zeiss LSM 710 confocal microscope, a Nikon eclipse fluorescence microscope, and ImageJ/FIJI software were used to capture and analyze images. Quantitation of cell numbers was completed using at least 10 randomly selected images per animal with at least 50 cells per image.

Antibodies

The following antibodies were used for immunostaining: rabbit polyclonal anti-ProSP-C (1:200, Millipore, AB3786), hamster monoclonal (8.1.1) anti-mouse T1α (1:200, Developmental Studies Hybridoma Bank, University of Iowa), goat polyclonal anti-GFP (1:200, Abcam, ab6673), rabbit polyclonal anti-RFP (1:250, Rockland, 600-401-379), rabbit monoclonal (SP6) anti-mouse Ki67 (1:100, Abcam, ab16667), mouse monoclonal (8D5) anti-mouse Ki67 (1:100, Cell Signaling Technology, 9449), rabbit polyclonal anti-ATF3 (1:50, ABclonal, A13469), rabbit polyclonal anti-THRA (1:25, Invitrogen, PA1-211A), chicken polyclonal anti-GFP (1:250, Aves Labs, GFP1020), rabbit monoclonal anti-mouse TTF-1/Nkx2-1 (1:250, Abcam, ab76013), mouse monoclonal anti-HOP (HOPX, 1:50, Santa Cruz, sc-398703), chicken anti-goat IgG (H + L) secondary antibody, Alexa Fluor 488 (1:500, Thermo Fisher Scientific, A-21467), goat anti-rabbit IgG (H + L) secondary antibody, Alexa Fluor 488 (1:500, Thermo Fisher Scientific, A-11008), goat anti-rabbit IgG (H + L) secondary antibody, Alexa Fluor 568 (1:500, Thermo Fisher Scientific, A-11011), goat anti-mouse IgG (H + L) secondary antibody, Alexa Fluor 568 (1:500, Thermo Fisher Scientific, A-11004), goat anti-hamster IgG (H + L) secondary antibody, Alexa Fluor 568 (1:500, Thermo Fisher Scientific, A-21112), rabbit anti-Chicken IgY (H + L) FITC conjugate (Jackson Immuno Research Lab, 303-095-003). TUNEL staining was performed using *In Situ* Cell Death Detection Kit (Roche). EdU incorporation assay was performed using Click-iT® EdU (5-ethynyl-2'-deoxyuridine) Alexa Fluor® Imaging Kit (ThermoFisher Scientific).

AT2 cell isolation for cell sorting by flow cytometry

Mouse AT2 cells were isolated following a previously described protocol (LaCanna et al., 2019). Briefly, lungs were inflated through the trachea with 3 mL of dispase (25 U/ml, 37°C) and 0.5 mL of 1% low melting agarose. After incubation with ice for 2 min, lungs were incubated in dispase for 6 min at 37°C. Lungs were then minced and digested in DNase I (120 U/mL) in DMEM for 10 min at room temperature. The cells were then filtered sequentially through 100- and 40- um strainers and centrifuged. The cells were incubated with red blood cell lysis buffer for 1 min on ice and washed with PBS containing 5% BSA and 0.5 M EDTA. Flow cytometry was performed on a BD LSR II and sorting was performed on a BD influx.

Single cell RNA-seq library preparation and sequencing

Single cell RNA-seq libraries were generated using Single Cell 3' Reagent Kits v2 (10xGenomics) according to the manufacturer's protocol. Briefly, the Chromium Single Cell A Chip (10xGenomics, 1000074) were loaded with cells, reagents (10xGenomics, PN-120237), gel beads (10xGenomics, 1000092), and partitioning oil (10xGenomics, 220088). cDNA was generated using the Gel Bead-In-Emusions (GEMs)-RT incubation protocol, purified with DynaBeads MyOne Silane beads, amplified with PCR, and further purified with SPRI-select reagent (Beckman Coulter, B23318). After fragmentation, end-repair, A-tailing and size purification, cDNA was ligated with adaptor, followed by quantification with SPRI-select reagents. Libraries were amplified using PCR with sample indexes from Chromium i7 Multiplex kit (10xGenomics, PN-120262). Library quality control was performed on the Agilent Tapestation with D1000 screen tapes, and library yield was quantified by Qubit DNA high sensitivity assay. Sequencing was performed on an Illumina

Nextseq 500 system operated by the Next Generation Sequencing at GENEWIZ using the HiSeq 2 × 150 bp high output sequencing kit.

Pre-processing of scRNA-seq data

The scRNAseq data was processed by Cell Ranger (v.3.0.2, 10X Genomics) followed by Seurat suite (version 4.0.1). Briefly, sample demultiplexing was performed based on sample index reads to generate FASTQ files for each sequencing library using Cell Ranger mkfastq mode, and then STAR aligner was used to map raw reads to the mouse genome (mm10) through the Cell Ranger count mode. Subsequently, the Seurat suite (version 4.0.1) was used to perform filtering, normalization, data scaling, and Principal component analysis (PCA) and Uniform Manifold Approximation and Projection (UMAP) analysis for dimensionality reduction and clustering (Stuart et al., 2019). Genes differentially expressed across clusters were identified using likelihood ratio test.

Motif enrichment analysis of differential accessible peaks

The 5-kb promoter sequences upstream of transcription start site (TSS) of DEGs between infected AT2 and naïve AT2 cells in Cluster 2 was extracted, and the homer suite was used to perform motif enrichment analysis with the findMotifsGenome perl script with the parameter "-len 6,8,10 -mis 2 -S 6 -preparse"

Cell-cycle analysis

Cell cycle analysis for individual AT2 cell in each cluster was performed using a published approach (Kowalczyk et al., 2015) (https://satijalab.org/seurat/v4.0/cell_cycle_vignette.html). Briefly, a list of genes associated with either S or G2/M cell-cycle phase was used to assign cell-cycle scores, an index of cell-cycle activity, based on the scaled expression of these genes in each cell.

AT2 cell *in vitro* proliferation assay

Mouse AT2 cells were isolated from 5- or 6-week-old mice following procedures described in "AT2 cell isolation for cell sorting by flow cytometry". After steps of dispase and DNase I treatment, isolated cells were filtered through 100 and 40 μm strainers and incubated with magnetic anti-CD45 MicroBeads from Miltenyi Biotec for 15 min at 4°C. Cells were passed through magnetic LS columns from Miltenyi Biotec and flow through was collected. Cells were then incubated with FcR Blocking Reagent from Miltenyl Biotech for 10 min and with anti-Mouse Biotin antibody for EpCAM from Invitrogen for 30 min at 4°C. Next, cells were incubated with streptavidin MicroBeads from Miltenyi Biotec for 20 min at 4°C. Cells were then passed through LS magnetic columns and flow through were discarded. Captured cells were then eluted as isolated AT2. Isolated mouse AT2 cells were plated at a density of 50000/cm^2 to rat tail collagen-coated plates and were maintained in culture medium with 2% fetal bovine serum. Culture medium composition is 0.25% bovine serum albumin, 1 mM L-glutamine, 10 mM HEPES, 0.1 mM nonessential amino acids, 0.05% insulin-transferrin-sodium selenite, 100 U/mL penicillin G, 100 μg/mL streptomycin in DMEM/F12 (1:1). At 24 hours after seeding, cells were infected with Ad-Cre, Ad-ATF3 and Ad-THRA at 100 MOI in culture medium for 48 hours. For proliferation assay, viral medium was replaced with culture medium containing 10 μM EdU. Sixteen hours later, cells were analyzed for staining or RNA isolation.

Bulk RNA sequencing in AT2 cells and data analysis

Mouse AT2 cells were collected at 48 hours after infection with adenoviruses for Cre, ATF3,and THRA. RNA was extracted and purified using RNeasy Mini Kit (QIAGEN, Catalog number 74104) following the manufacturer's protocol. An Agilent Bioanalyzer was used for RNA quality analysis. RNA libraries were prepared using NEBNext® Ultra™ II RNA Library prep kit. RNA sequencing was performed by the Next Generation Sequencing core of Fox Chase Cancer Center at Temple University Health System. The Illumina Nextseq 500 system was used to generate raw data at 75 cycles. Fastq files was aligned to the reference genome mm10 and DEseq2 was used to analyze the differentially expressed genes. Gene oncology (GO) associations and related p values were determined using ToppGene Suite (de Hoon et al., 2004) (https://toppgene.cchmc.org).

Generation of adenovirus (Ad) and AAV

Ad-ATF3 (Catalog number ADV-253206) was purchased from Vector Biolabs. Ad-THRA (Catalog number 466670540200), AAV6-ATF3-GFP (Catalog number 126091040216), and AAV6-THRA (Catalog number

466671040116) were purchased from Applied Biological Materials Inc. Ad-Cre and AAV6-GFP were gifts from Dr. Joseph Rabinowitz.

Intratracheal injection of AAV6

The procedure was performed according to previously described (7). Mice were anesthetized by inhalation of isoflurane. AAV6-ATF3-GFP, or AAV6-THRA, or AAV6-GFP diluted in 50 ul of sterile saline was instilled intratracheally via a 23G cannula. The dose was 1.5×10^{10} vp/animal.

Quantitative real-time PCR analysis

RNA for real-time PCR were extracted using Trizol from cultured mouse AT2 cells. cDNA was produced using random hexamer primers and Super- Script III RT (Invitrogen). Real-time PCR was performed using StepOne Plus cycler (Applied Biosystems) with SYBR green master mix. Comparative threshold cycle (Delta CT) method was used to transcript expression values and normalize to the expression of GAPDH gene. Sequences of the oligonucleotide primers used for qRT-PCR analysis are: *Anln, forward: 5′-GTAATCAGCAG CAGCCCCTA-3′, reverse: 5′-CGGAGCTCCCACTTCAATTT-3′; Ect2, forward: 5′-CAGTGCAGAGGCTA CCCAGT-3′, reverse: 5′-GGATTTTCATCAGCTGTATGCTTT-3′; Aurkb, forward: 5′-AGATTGCAGACTTTG GCTGG-3′, reverse: 5′-AATCATCTCTGGGGGCAGAT-3′; Birc5, forward: 5′-AAGGAATTGGAAGGC TGGG-3′, reverse: 5′-TTCTTGACAGTGAGGAAGGC-3′; Plk1, forward: 5′-AGCAGCAGGAAACCTCTCA A-3′, reverse: 5′-GACCACCGGTTCCTCTTTCT-3′; Dapk1, forward: 5′-GCTGAACATGGAGCTGACTT-3′, reverse: 5′-CAAGGAGGGTCTTGATGACTTC-3′; Stk17b, forward: 5′-AATCTGCATGAGGTCTACGAAA-3′, reverse: 5′-TCGGCTAACTCAGGTAAACAC-3′; Trp53, forward: 5′-AAAAGAGTGCGCCGATAGGT-3′, reverse: 5′-ATCCGACTGTGACTCCTCCA-3′; Atf3, forward: 5′-GCCAAGTGTCGAAACAAGAA-3′, reverse: 5′-CCGGTGCAGGTTGAGCATGTAT-3′; Thra, forward: 5′-CCTGGACAAAGACGAGCAGTGT-3′, reverse: 5′-CTGGATTGTGCGGCGAAAGAAG-3′; 18s, forward: 5′-TCAAGAACGAAAGTCGGAGG-3′, reverse: 5′-GGACATCTAAGGGCATCAC-3′.*

QUANTIFICATION AND STATISTICAL ANALYSIS

Statistical analyses were performed using GraphPad Prism 9 (GraphPad Software Inc). All data are displayed as mean $\pm$ SEM(SEM). Multiple groups were compared by one-way ANOVA followed Tukey or Dunnett's post hoc test. Student's t test was used when comparing two experimental groups. A p value less than 0.05 is considered significant. p values were displayed as follows: $*p < 0.05$; $**p < 0.01$; $***p < 0.001$; $****p < 0.0001$. Results with $p > 0.05$ were considered not significant (*n.s.*).